

Manuscript Number: CARBPOL-D-15-03487R1

Title: PLLA-grafted cellulose nanocrystals: role of the CNC content and grafting on the PLA bionanocomposite film properties

Article Type: Research Paper

Keywords: Poly(lactic acid); cellulose nanocrystals; grafting; renewable bionanocomposites; interfacial compatibility.

Corresponding Author: Dr. Ilaria Armentano,

Corresponding Author's Institution: University of Perugia

First Author: Erlantz Lizundia

Order of Authors: Erlantz Lizundia; Elena Fortunati; Franco Dominici; José Luis Vilas; Luis Manuel Leon; Ilaria Armentano; Luigi Torre; José M Kenny

Abstract: Cellulose nanocrystals (CNC), extracted from microcrystalline cellulose by acid hydrolysis, were grafted by ring opening polymerization of L-Lactide initiated from the hydroxyl groups available at their surface and two different CNC:L-lactide ratios (20:80 and 5:95) were obtained. The resulting CNC-g-PLLA nanohybrids were incorporated in poly(lactic acid) (PLA) matrix by an optimized extrusion process at two different content (1 wt.% and 3 wt.%) and obtained bionanocomposite films were characterized by thermal, mechanical, optical and morphological properties. Thermal analysis showed CNC grafted with the higher ratio of lactide play a significant role as a nucleating agents. Moreover, they contribute to a significant increase in the crystallization rate of PLA, and the best efficiency was revealed with 3wt.% of CNC-g-PLLA. This effect was confirmed by the increased in Young's modulus, suggesting the CNC graft ratio and content contribute significantly to the good dispersion in the matrix, positively affecting the final bionanocomposite properties.

1

2 **Highlights**

- 3 1. Bionanocomposite films were developed by an optimized extrusion process
- 4 2. Cellulose nanocrystals (CNC) were grafted by ring opening polymerization of L-Lactide
- 5 3. Two different CNC:L-lactide ratios (20:80 and 5:95) were obtained
- 6 4. CNC grafted with the higher ratio of lactide act as a nucleating agents
- 7 5. CNC graft ratio and content influence all the final bionanocomposite properties.

8

1 **PLLA-grafted cellulose nanocrystals: role of the CNC content and grafting on**
2 **the PLA bionanocomposite film properties**

3 Erlantz Lizundia,¹ Elena Fortunati^{2*}, Franco Dominici², José Luis Vilas,^{1,3} Luis Manuel León^{1,3},
4 Ilaria Armentano^{2*}, Luigi Torre², Josè M. Kenny²

5 ¹*Macromolecular Chemistry Research Group (LABQUIMAC). Dept. of Physical Chemistry.*
6 *Faculty of Science and Technology. University of the Basque Country (UPV/EHU), Leioa 48940,*
7 *Spain.*

8 ²*University of Perugia, Civil and Environmental Engineering Department, UdR INSTM, Strada di*
9 *Pentima 4, 05100 Terni, Italy.*

10 ³*Basque Center for Materials, Applications and Nanostructures (BCMaterials), Parque*
11 *Tecnológico de Bizkaia, Ed. 500, Derio 48160, Spain.*

12 **Corresponding Authors: Ilaria Armentano, ilaria.armentano@unipg.it*

13 *Elena Fortunati, elena.fortunati@unipg.it*

14

15 **Abstract**

16 Cellulose nanocrystals (CNC), extracted from microcrystalline cellulose by acid hydrolysis, were
17 grafted by ring opening polymerization of L-Lactide initiated from the hydroxyl groups available at
18 their surface and two different CNC:L-lactide ratios (20:80 and 5:95) were obtained. The resulting
19 CNC-g-PLLA nanohybrids were incorporated in poly(lactic acid) (PLA) matrix by an optimized
20 extrusion process at two different content (1 wt.% and 3 wt.%) and obtained bionanocomposite
21 films were characterized by thermal, mechanical, optical and morphological properties. Thermal
22 analysis showed CNC grafted with the higher ratio of lactide play a significant role as a nucleating

1 agents. Moreover, they contribute to a significant increase in the crystallization rate of PLA, and the
2 best efficiency was revealed with 3wt.% of CNC-g-PLLA. This effect was confirmed by the
3 increased in Young's modulus, suggesting the CNC graft ratio and content contribute significantly
4 to the good dispersion in the matrix, positively affecting the final bionanocomposite properties.

5 **Keywords:** Poly(lactic acid); cellulose nanocrystals; grafting; renewable bionanocomposites;
6 interfacial compatibility.

7

81. Introduction

9 Polylactides (PLAs) have been known for several decades but only recently they have gained
10 commercial significance as a leading environmentally benign plastic available from renewable
11 resources (Armentano et al., 2013). Besides of their bio-based character, they exhibit an excellent
12 melt-processability, good biodegradability/biocompatibility, a room-temperature elastic modulus
13 comparable to poly(ethylene terephthalate) and tunable crystallinity (Liu, Zhang, & Wang, 2014;
14 Obarzanek-Fojt et al., 2014; Lizundia, Petisco, & Sarasua, 2013), which make them particularly
15 interesting for the development of green materials (Auras, & Selke, 2004). More precisely, the use
16 of poly(lactic acid) in packaging applications would contribute to the reduction of the
17 environmental impact associated with the massive use of traditional plastics based on petrochemical
18 resources.

19 However, some of its functional properties still remain insufficient for their commercialization for
20 food packaging and container applications. A possible solution to this matter may come from
21 synergetic effect achieved when polymer matrices are mixed with nanoscale particles (Paul, &
22 Robeson, 2008; Armentano et al., 2013). In the aim of producing fully organic bionanocomposite
23 based on poly(lactic acid) (PLA), cellulose nanocrystals (CNC) could be dispersed into PLA
24 polymer matrix. CNC are large surface area **nanoparticles based on cellulose**, which represents the
25 most abundant naturally available polymer on the Earth (Xiao, Gao, Lu, Li, & Sun, 2015). **The**

1 **CNC properties make them ideal for mechanical reinforcing purposes.** Dispersion and distribution
2 of cellulose nanocrystals in a thermoplastic matrix is one of the most important issues in the
3 development of CNC based high performance composites (Arias, Heuzey, Huneault, Ausias, &
4 Bendahou, 2015). In this sense, when CNC are introduced within non-polar polymers such as PLA,
5 they **tend** to bundle together due to the occurring intra- and inter-molecular hydrogen bonds
6 between adjacent cellulose chains, which notably limits their efficiency as reinforcing elements
7 (Dufresne, 2013). Furthermore, CNC show poor compatibility with hydrophobic polymer matrices
8 because of the dominant hydrophilic nature of cellulose (Song, Xiao, & Zhao, 2014), which yields
9 an inefficient transfer of CNC properties to its hosting matrix. **Different strategies are available to**
10 **solve this problem** (Habibi, 2014; Lizundia, Vilas, & León, 2015; Bitinis, et al., 2013; Habibi,
11 Aouadi, Raquez, & Dubois, 2013; Spinella, et al., 2015; Fortunati, et al., 2012a;. Fortunati, et al.,
12 2012b).

13 The chemical grafting of determined moieties on CNC surface would decrease the surface energy of
14 the nanoparticle while increases the filler/matrix compatibility (Dufresne, 2013). Between all the
15 techniques that are currently being employed, the polymer grafting known as “grafting from”
16 strategy shows the brighter future. Taking advantage of the numerous surface hydroxyl groups of
17 cellulose and the well-known ring-opening polymerization of polyesters (Dechy-Cabaret, Martin-
18 Vaca, & Bourissou, 2004), surface-initiated ring opening polymerization (SI-ROP) emerges as the
19 most suitable technique to overcome dispersion and compatibility issues associated with the
20 development of PLLA/CNC nanocomposites. This method presents the additional advantage of
21 allowing the development of high grafting densities and controlled grafted chain lengths together
22 with respecting the structural integrity of starting cellulose nanocrystals (Goffin, et al. 2011).
23 Another remarkable advantage of this method is that it permits the addition of dried CNC directly to
24 the melt polymer, which represents an almost essential requirement towards the development of
25 solvent-free industrially-scalable fabrication process.

1 The goal of the present work **consists of** improving the interfacial compatibility within CNC and
2 hydrophobic PLA matrix in order to develop well dispersed and fully renewable bionanocomposites
3 film by using an industrial process technology. The role of the CNC grafting and its ratio and CNC-
4 g-PLLA nanohybrid content added to the PLA, were investigated by a detailed investigation of
5 physical and chemical properties of the obtained PLA based systems.

72. **Material and Methods**

8 **2.1. Materials**

9 L-lactide monomer (assay >99.5%) with <0.02 % of water content was provided by Purac Biochem
10 (The Netherlands). Stannous octoate ($\text{Sn}(\text{Oct})_2$) and microcrystalline cellulose were supplied by
11 Sigma Aldrich[®]. The chloroform and acetone were purchased from LabScan and utilized without
12 further purification. Methanol was purchased by Panreac. Commercial poly(lactic acid) PLA
13 3251D, was **purchased by** NatureWorks[®] Co. LLC, USA. This PLA grade shows specific gravity
14 1.24 g/cm^3 , and a melt flow rate (MFR) of 80 g/10 min tested at 210 °C and 2.16 kg loading.

16 **2.2. Cellulose nanocrystals synthesis and grafting**

17 Cellulose nanocrystals (CNC) were obtained by sulfuric acid hydrolysis of microcrystalline
18 cellulose as previously described (Lizundia, Vilas & León., 2015, Fortunati, et al., 2012a;
19 Fortunati, et al., 2012b). Grafting of PLLA from synthesized CNC has been performed by surface-
20 initiated ring opening polymerization (SI-ROP) of L-lactide. Firstly, water-dispersed CNC were
21 exchanged to toluene through several steps using acetone as an intermediate solvent as previously
22 reported (Lizundia, Vilas & León., 2015). The CNC/toluene suspension was introduced into a three-
23 neck flask immersed in a controlled temperature oil bath at 80 °C. The required amount of
24 previously dissolved L-lactide **in toluene** was poured into CNC suspension and ($\text{Sn}(\text{Oct})_2$) was

1 added using a 100:1 monomer to catalyst ratio. Polymerization has been carried out for 24 h and
2 was stopped by adding a few drops of diluted HCl solution. The resulting product was then
3 precipitated in an excess of cold methanol and dried at 60 °C under vacuum for 72 h. Obtained
4 nanohybrids are termed as CNC-g-PLLA1 and CNC-g-PLLA2 for a CNC:L-lactide ratios of 20:80
5 and 5:95, which falls in the typical range utilized up to date (Goffin, et al. 2011).

6

7 **2.3. Characterization of CNC-g-PLLA nanohybrids**

8 Cellulose nanocrystals were examined by transmission electron microscopy (TEM) using a Philips
9 CM120 Biofilter apparatus with STEM module at an acceleration voltage of 120 kV. A droplet of
10 cellulose diluted water suspension (0.1 % (w/w)) was deposited on hydrophilic carbon-coated grids
11 and the specimens were negatively stained with 1 % uranyl acetate ($\text{UO}_2(\text{CH}_3\text{COO})_2$) for 1 min and
12 then observed **using TEM**. Infrared spectra in transmission KBr mode were recorded on a Thermo
13 Nicolet Nexus 670 Fourier transform infrared spectrophotometer (FT-IR). Samples were dried in
14 vacuum at 60 °C for 24 h before characterization. Each IR spectrum consisted of 64 scans taken in
15 the range 600–4000 cm^{-1} with a resolution of 1 cm^{-1} .

16 The thermal behavior of CNC-g-PLLA nanohybrids was determined by using a Mettler Toledo
17 DSC 822e calorimeter under nitrogen atmosphere (30 mL/min). Samples of 8 ± 1 mg were sealed in
18 an aluminum pan, heated from -20 °C to 170 °C at a rate of 10 °C/min in order to determine thermal
19 transitions (T_g and T_m) and held at 170 °C for 2 min so as to ensure that the previous thermal history
20 is removed. After quenching the samples down to -20 °C, a subsequent heating scan at 10 °C/min
21 was applied to the samples in order to determine the glass transition, cold crystallization and
22 melting temperatures and enthalpies (T_g , T_{cc} , and T_m , ΔH_{cc} , ΔH_m). Thermal degradation behavior
23 was studied by means of thermal gravimetric analysis (TGA METTLER TOLEDO 822e) in
24 alumina pans with nitrogen flux of 50 mL/min for each sample (8 mg).

25

1 **2.4. Processing of PLA_CNC-g-PLLA bionanocomposite films**

2 PLA and PLA based bionanocomposites were processed and mixed by using a twin-screw
3 microextruder (Dsm Explore 5&15 CC Micro Compounder). Processing parameters (screw speed,
4 mixing time and temperature profile) were modulated to optimize the extrusion procedure. PLA
5 pellets and CNC-g-PLLA nanohybrids were pre-dried to get rid of any moisture trace in the
6 polymer structure and to avoid any undesirable hydrolysis reaction during processing. PLA was put
7 into an oven at 98 °C for 3 h, while CNC were dried overnight at 37 °C. PLA and cellulose based
8 films with thicknesses between 20 and 60 µm were obtained with the adequate filmature die. Screw
9 speed at 100 rpm was used to optimize the material final properties, while the temperature profile
10 was set up at 180-195-210 °C in the three different extrusion areas. The selected contents of CNC-
11 g-PLLA (both CNC-g-PLLA1 and CNC-g-PLLA2) were 1 wt.% (designed PLA_1CNC-g-PLLA1
12 or PLA_1CNC-g-PLLA2) and 3 wt.% (designed as PLA_3CNC-g-PLLA1 or PLA_3CNC-g-
13 PLLA2), in PLA polymer matrix.

14

15 **2.5. PLA_CNC-g-PLLA bionanocomposite characterization**

16 **2.5.1. Microstructure**

17 The morphology and microstructure of the fracture surfaces of PLA and PLA bionanocomposite
18 films were analyzed in a Hitachi S-4800 field emission scanning electron microscope (FESEM) at
19 an acceleration voltage of 5 kV. Films were previously freeze-cut in liquid nitrogen, gold coated by
20 an Emitech K550X sputter coater.

21 **2.5.2. Optical absorption, gloss and color determination**

22 The transparency of films was evaluated by visual observation and UV-VIS optical absorption
23 measurements, by using a Perkin Elmer Instruments (Lambda 35, USA) spectrophotometer,
24 working in the wavelength between 250 and 900 nm. Color values were determined by using a

1 spectrophotometer (CM-2300d Konica Minolta, Japan). Data were acquired by using a diffused
2 illumination with a 8° viewing system (D/8 geometry) conforming to CIE N.15 and ISO 7724/1
3 standards. The measurement conditions were selected with the following standard parameters:
4 observer at 10° (CIE 1964), illuminant D65 (Daylight, Color temperature 6504 K), while CIELAB
5 colour variables, as defined by the Commission Internationale de l'Éclairage (CIE 1995), were used
6 (CIE, 1995). Film specimens were placed on a white standard plate and L*, a*, and b* parameters
7 were determined. Samples were evaluated per triplicate and three measurements were taken at
8 random locations on each of the studied films. The total color difference ΔE, between PLA and
9 PLA bionanocomposite films was calculated as follows:

$$\Delta E = \sqrt{(\Delta L^*)^2 + (\Delta a^*)^2 + (\Delta b^*)^2} \quad (1)$$

11 where L is the luminance component, which ranges from 0 to 100, and parameters a (from green to
12 red) and b (from blue to yellow) are the two chromatic components, which range from -120 to 120,
13 and ΔL, Δa, and Δb are differences between each color value of the standard color plate and film
14 specimen, respectively.

15 Gloss of PLA and PLA bionanocomposite films was determined considering the Specular
16 Component Included with a diameter of the measurement area of 8 mm (SCI 8).

17 2.5.3 Thermal analysis

18 Differential scanning calorimetry (DSC -TA Instrument, Q200) measurements of PLA_CNC-g-
19 PLLA bionanocomposites were performed in the temperature range from -25 to 210°C at 10°C/min
20 under nitrogen flow. PLA and PLA bionanocomposite samples (6–7 mg) were heated from -25 to
21 210 °C at a rate of 10°C/min and held at 210 °C for 2 min to erase the thermal history (1stscan), then
22 they were cooled to -25 at 10 °C/min (cooling) and reheated under the same conditions (2ndscan).
23 Glass transition (T_g), cold crystallization (T_{cc1} and T_{cc2}) and melting (T_m) temperatures and
24 enthalpies (ΔH_{cc1} , ΔH_{cc2} , ΔH_m) were determined from the first and second heating scans. The

1 crystallinity degree (χ) was calculated from the heating scans as:

$$2 \quad \chi = \frac{\Delta H_m - \Delta H_{cc}}{\Delta H_0(1 - m_f)} \times 100 \quad (2)$$

3 and from the cooling as:

$$4 \quad \chi = \frac{\Delta H_c}{\Delta H_0(1 - m_f)} \times 100 \quad (3)$$

5 where ΔH_0 is enthalpy of melting for a 100% crystalline PLA sample, taken as 93J/g (Martin, &
6 Avérous, 2001), $(1 - m_f)$ is the weight fraction of PLA matrix in the sample, ΔH_m and ΔH_{cc} are the
7 melting and cold crystallization enthalpies calculated from the first heating scan while the ΔH_c is
8 the crystallization enthalpy calculated from the cooling.

9 Thermodegradation products analysis has been performed by using a Fourier Transform Infrared
10 Spectrophotometer (FT-IR) connected through an interface to DTG-60 Shimadzu thermobalance.
11 Samples were heated from room temperature to 500 °C at 10 °C/min under nitrogen atmosphere.
12 FT-IR scans were taken every 16 s.

13

14 2.5.4. Wide angle X-ray diffraction (WAXD)

15 The X-ray powder diffraction patterns were collected in a PHILIPS X'PERT PRO automatic
16 diffractometer in theta-theta configuration, secondary monochromator with Cu-K α radiation (λ
17 =1.5418 Å) and a PIXcel solid state detector. The sample was mounted on a zero background
18 silicon wafer fixed in a generic sample holder. Data were collected from 5 to 40 ° 2θ (step size =
19 0.026) at RT.

20

21 2.5.5. Chemical analysis

1 Fourier Transform Infrared Spectroscopy (FT-IR) spectra of the PLA and PLA bionanocomposite
 2 films were obtained at room temperature in reflection mode by attenuated total reflectance (ATR),
 3 with a FT-IR spectrometer (Jasco FT-IR 615, Japan). The scanned wavenumber range was 4000-
 4 600 cm^{-1} , at 4 cm^{-1} of spectral resolution.

6 2.5.6. Mechanical analysis

7 The mechanical response of PLA and PLA bionanocomposites was evaluated by tensile test
 8 according to the European Standard EN ISO 527-3:1995. Before testing, samples were conditioned
 9 at 22°C and 51%RH **overnight**. Experiments were carried out on a AGS-X Universal Testing
 10 Machine from Shimadzu at 5mm/min by using 50mm long and 10mm width specimens. Young's
 11 modulus (E) (calculated from slope of a secant line between 0.5 and 1% strain on stress-strain plot),
 12 stress and strain at yield (σ_y and ε_y respectively) and stress and strain at break (σ_b and ε_b
 13 respectively) were determined. Reported values represent mean average value and standard
 14 deviation over 5 specimens. **Experimentally obtained tensile modulus could be compared with**
 15 **theoretical predictions by using a modified Halpin-Tsai model as (Halpin, & Kardos, 1976; Hui, &**
 16 **Shia, 1998):**

$$17 \quad \frac{E_c}{E_m} = \left(\frac{3}{8} \right) \left(\frac{1 + 2\rho\eta_L V_{CNC}}{1 - \eta_L V_{CNC}} \right) + \left(\frac{5}{8} \right) \left(\frac{1 + 2\eta_T V_{CNC}}{1 - \eta_T V_{CNC}} \right) \quad (4)$$

$$18 \quad \eta_L = \frac{E_r - 1}{E_r + 2\rho} \quad \eta_T = \frac{E_r - 1}{E_r + 2} \quad (5)$$

19 **where E_c and E_m are the Young's modulus of the composite and matrix respectively, ρ is the CNC**
 20 **aspect ratio, V_{CNC} is its volume fraction within the bionanocomposite and E_r is defined as the ratio**
 21 **between the Young's modulus of the filler and the matrix. CNC volume fractions have been**
 22 **calculated from the weight fraction of both components and their densities, assuming a density of**

1 1.25g/cm³ for PLA and 1.676g/cm³ for cellulose nanocrystals (Diddens, Murphy, Krisch, & Muller,
2 2008), while the Young's modulus of CNC-g-PLLA nanoparticles has been set at 105 GPa (Rusli,
3 & Eichhorn, 2008).

4

53. Results and Discussion

6 3.1. CNC-g-PLLA nanohybrids characterization

7 Morphological, physico-chemical and conformational characterization of synthesized raw CNC and
8 CNC-g-PLLA nanohybrids have been carried out as highlighted in Fig. 1. TEM micrograph shown
9 in Fig. 1a presents rod-shaped well-individualized cellulose nanocrystals having a length of
10 150±60nm and width of about 9-17 nm (particle size distribution has been calculated from 8 TEM
11 images). Conformational features of CNC grafted with PLLA were analyzed by FT-IR. Absorbance
12 spectra corresponding to raw CNC, CNC-g-PLLA1 and CNC-g-PLLA2 are plotted in Fig. 1b, while
13 the spectra of commercially available microcrystalline cellulose, L-lactide and medium molecular-
14 weight poly(L-lactide) are provided for comparison (characteristic bands of cellulose, L-lactide and
15 poly(L-lactide) are vertically expanded by a dashed line with ►, † and X ends respectively).
16 Synthesized CNC show the characteristic O-H stretching vibration broad band at 3650-3200 cm⁻¹
17 and a narrower band centered at 2902 cm⁻¹ corresponding to the stretching of asymmetric and
18 symmetric methyl and methylene C-H groups (Kondo, & Sawatari, 1996). Further bands assigned
19 to the C-O-H in plane bending, C-O-C bending and C-O-C asymmetric stretching at the B-
20 (1→4)-glycosidic linkage are achieved at 1337 cm⁻¹, 1160 cm⁻¹ and 897 cm⁻¹ respectively (Colom,
21 & Carrillo, 2002). A crystallinity degree of 52.9 % is determined for employed CNC according to
22 the $A_{1431,1419}/(A_{1431,1419} + A_{897,894})$ ratio (Oh, et al. 2005; Lizundia, Vilas, & León, 2015). PLLA
23 grafting on CNC surfaces is proved by the presence of the characteristic absorption bands of PLLA
24 (CH₃ group stretching at 3017 cm⁻¹, C=O stretching vibration at 1760 cm⁻¹, in plane deformation at
25 1458 cm⁻¹, rocking vibration at 1187 cm⁻¹) (Goncalves, Cuntinho, & Marrucho, 2010; Meaurio,

1 Martinez de Arenaza, Lizundia, & Sarasua, 2009), together with the broad O-H stretching band of
2 cellulose for CNC-g-PLLA1 and CNC-g-PLLA2. Additionally, the relative 3650-3200 cm^{-1}
3 (cellulose O-H) and 1760 cm^{-1} (PLLA C=O stretching) peak height indicates that the CNC-to-
4 PLLA ratio is significantly higher for CNC-g-PLLA1 nanohybrid. Results demonstrate that no
5 traces of L-lactide remain in any of the synthesized nanohybrids.

6 Fig. 1c. displays the heating differential scanning calorimetry traces for both CNC-g-PLLA1 and
7 CNC-g-PLLA2 nanohybrids. Although CNC-g-PLLA1 does not suffer any thermal transition
8 within the studied temperature range suggesting that a very small fraction of grafted PLLA, CNC-g-
9 PLLA2 presents several thermal transitions associated with the glass transition (heat enthalpy
10 change located at 47.8 °C), cold crystallization (exothermic peak at 78.3 °C) and melting of grafted
11 PLLA chains (at 158 °C) (Lizundia, Petisco, & Sarasua, 2013). The low T_g , T_{cc} and T_m values
12 measured for CNC-g-PLLA2 evidence the low molecular weight of grafted chains for this
13 nanohybrids (Lizundia, Meaurio, Laza, Vilas, & León, 2015). Additionally, the thermal stability of
14 raw CNC and both synthesized nanohybrids, has been evaluated by thermogravimetric analysis
15 under nitrogen atmosphere (TGA trace corresponding to L-lactide is shown as reference, Fig. 1d).
16 Thermal degradation of raw CNC, which is due to the depolymerization, dehydration and
17 decomposition of cellulosic glycosyl units (Roman, & Winter, 2004) starts at 270.2 °C and reaches
18 its maximum value (T_{max}) at 332.9 °C. On the contrary, CNC-g-PLLA1 thermodegradation takes
19 place at lower temperatures ($T_{max}=311.6$ °C), while CNC-g-PLLA2 degrades at similar temperatures
20 than raw CNC. The reduced thermal stability of CNC-g-PLLA1 originates from the presence of
21 residual tin compound arising from SI-ROP process, which boosts the thermodegradation process of
22 nanohybrids (Lizundia, Vilas, & León, 2015). The amount of char residue at 400 °C indicates that
23 the CNC-to-PLLA ratio within nanohybrids is much larger in CNC-g-PLLA1 nanohybrid in
24 comparison with CNC-g-PLLA2.

25

1 **3.2. PLA_CNC-g-PLLA bionanocomposite films**

2

3 **3.2.1. Morphological analysis**

4 Fig. 2 shows the FESEM images of the cryogenic fractured surfaces of neat PLA and PLA based
5 bionanocomposite films at different magnifications. Neat PLA showed a smooth and uniform
6 surface typical of a semicrystalline polymer, as previously observed (Yang, Dominici, Fortunati,
7 Kenny, J.M., & Puglia, 2015). A similar behavior was also observed for PLA_1CNC-g-PLLA1
8 bionanocomposites, underlining a good dispersion of these cellulose nanocrystals in the polymer
9 matrix. On the other hand, the surfaces of specimens with different content of CNC-g-PLLA2
10 showed a different microstructure: at lower concentration (1 wt.%) samples showed relatively small
11 domains with a typical sea-island morphology, while increasing the CNC content (3 wt.%) some
12 aggregates were evident.

13

14 **3.2.2. Optical properties**

15 Optical properties, UV-VIS spectra, colorimetric analysis and gloss of the films are directly related
16 with their nano- and micro-structure.

17 The transparency of the produced PLA based films was evaluated by UV-VIS optical absorption
18 measurements, in the visible range (400-800 nm). According to ASTM D1746-03, which
19 determines the transparency of plastics as the transmission of the light in the 540-560 nm range,
20 fabricated films present a transparency of 93-95% (spectra do not shown). The absorption and
21 transmission of light by polymer films is an important property in many industrial applications, as
22 in the food packaging industry, where the packaged goods are light sensitive (Turhan, & Sahbaz,
23 2001). In the fresh food packaging, an important issue is the effect of irradiation in the package
24 since ultraviolet light irradiation is a common method used for lowering microbial population in

1 foods. The spectrum and the intensity of the light source, the conditions of light exposure, and the
 2 degree of light transmittance of the packaging material are factors that can dramatically affect the
 3 food quality. Furthermore the color variation and gloss have to be considered in order to obtain new
 4 materials for food packaging application.

5 Apparent color and gloss, of PLA and PLA bionanocomposite films are shown in **Table 1**. *L*-value
 6 did not change appreciably after formation of bionanocomposite: the total color difference (ΔE) of
 7 both bionanocomposite films increased compared to neat PLA film. The most significant changes in
 8 color were found for PLA_3CNC-g-PLLA2 formulation. Gloss is a measurement of the ability of a
 9 surface to reflect direct light. As can be seen, gloss values decreased with CNC introduction. The
 10 gloss of the films is linked to the morphology of their surface and to the dispersion and aggregation
 11 of nanostructure in the polymer matrix (Sonjui, & Jiratumnukul, 2014). It is observed that PLA
 12 losses a gloss with the CNC addition. This effect is mainly evident with CNC-g-PLLA2, which
 13 should be expected due to the lactide units and CNC distribution. Gloss of both nanocomposite
 14 films was significantly lower than neat PLA film. The CNC modifications made possible the
 15 retention of the high original gloss (~129), while the increase of the CNC content dramatically
 16 reduce PLA gloss to 60.

17 **Table 1.** Apparent color, gloss and mechanical properties of PLA and PLA bionanocomposite films.

<i>Formulations</i>	<i>L*</i>	<i>a*</i>	<i>b*</i>	ΔE^*	<i>Gloss</i>	<i>E</i> (MPa)	ϵ_y (%)	σ_y (MPa)	ϵ_b (%)	σ_b (MPa)
<i>PLA</i>	93.57±0.09	3.86±0.08	15.76±0.09	-	137±5	1980 ± 230	2.6 ± 0.1	41 ± 7	5.6 ± 0.6	37 ± 8
<i>PLA_1CNC-g-PLLA1</i>	93.04±0.06	3.70±0.08	14.86±0.08	1.1±0.1	124±5	1960 ± 150	2.8 ± 0.2	41.9 ± 1.4	9.5 ± 0.9	36 ± 4
<i>PLA_3CNC-g-PLLA1</i>	92.93±0.09	3.62±0.08	14.09±0.08	1.8±0.1	65±6	2170 ± 240	2.5 ± 0.1	43 ± 4	4.4 ± 0.4	40 ± 4
<i>PLA_1CNC-g-PLLA2</i>	93.30±0.20	3.83±0.08	15.4±0.4	0.5±0.3	85±9	2200 ± 130	2.4 ± 0.1	43 ± 6	3.4 ± 0.5	37.5 ± 1.6
<i>PLA_3CNC-g-PLLA2</i>	95.56±0.06	3.58±0.08	13.74±0.08	2.3±0.1	96±7	2430 ± 170	2.1 ± 0.2	43.5 ± 1.5	2.2 ± 0.3	37.6 ± 1.5

18

19 **3.2.3. Thermal Properties**

20 Differential scanning calorimetry was used to investigate the glass transition, crystallization and
 21 melting phenomena of PLA and PLA bionanocomposites and study the effect of CNC addition,
 22 **grafting** and content on the final properties of the produced PLA based formulations. DSC

1 thermograms during first heating, cooling and second heating scan are shown in Fig. 3 while the
2 thermal properties obtained during the **first and second** heating scans are summarized in Table 2.
3 The glass transition temperatures, crystallization and melting phenomena of the bionanocomposites
4 did not change significantly respect to the PLA polymer matrix during the first heating scan (Fig.
5 3a.). Only the PLA_3CNC-g-PLLA2 formulation showed a shift to lower temperature of the T_{cc1} of
6 about 10°C with an increase in the crystallinity degree values (PLA= (12.8±1.8)%, PLA_3CNC-g-
7 PLLA2 = (18.6±1.5)%) that underlined the effect of this graft type and the best efficiency of the
8 highest content of CNC-g-PLLA2 (3wt.%). The effectiveness of CNC-g-PLLA2 at 3wt.% was also
9 confirmed during the cooling scan were the crystallization phenomenon was evident for
10 PLA_3CNC-g-PLLA2 formulation with an enthalpy value of (32.5±2.3)J/g respect to the
11 (3.2±0.3)J/g of neat PLA. These results are in agreement with the WAXD analysis, as would be
12 shown later. Finally, also during the second heating scan, the PLA_3CNC-g-PLLA2
13 bionanocomposite showed the highest value of crystallinity degree (39.6%) while the different
14 ability to re-crystallize after the cooling was highlighted by the low values of the first cold
15 crystallization enthalpy (ΔH_{cc1} = 6.7J/g respect to 28.7J/g of the neat PLA) and the absence of the
16 second cold crystallization enthalpy registered for this system.

17
18 **Table 2:** Thermal properties from DSC analysis of PLA and PLA bionanocomposite films from the first and the second
19 heating scan.

<i>Formulations</i>	$T_g(^{\circ}C)$	$\Delta H_{cc1}(J/g)$	$T_{cc1}(^{\circ}C)$	$\Delta H_{cc2}(J/g)$	$T_{cc2}(^{\circ}C)$	$\Delta H_m(J/g)$	$T_m(^{\circ}C)$	X_c (%)
FIRST HEATING SCAN								
PLA	58.7±0.7	32.5±3.2	102.6±0.3	1.6±0.2	156.3±0.5	46.1±3.2	169.1±0.6	12.8±1.8
PLA_1CNC-g-PLLA1	58.6±2.3	32.6±0.7	101.8±0.8	1.7±0.1	156.3±0.1	45.9±0.1	168.4±1.2	12.6±0.6
PLA_3CNC-g-PLLA1	57.6±0.8	31.6±0.8	99.0±1.0	3.0±0.1	154.6±0.5	48.6±0.5	168.7±0.9	15.6±0.2
PLA_1CNC-g-PLLA2	58.8±0.5	34.2±0.3	99.1±0.1	3.4±0.3	154.2±0.4	48.8±0.3	168.3±0.4	12.2±0.4
PLA_3CNC-g-PLLA2	57.1±0.3	32.0±0.8	92.5±0.3	3.3±0.2	153.2±0.3	51.8±0.5	167.0±0.8	18.6±1.5

	<i>SECOND HEATING SCAN</i>							
<i>PLA</i>	60.4±0.4	28.7±2.3	100.5±0.5	2.4±0.3	15.8±0.7	46.2±0.3	168.7±0.4	16.3±2.4
<i>PLA_1CNC-g-PLLA1</i>	59.9±0.3	29.0±0.3	100.5±0.2	2.3±0.1	154.0±0.1	47.9±1.0	167.6±0.7	18.1±0.8
<i>PLA_3CNC-g-PLLA1</i>	59.8±1.0	28.8±0.7	99.2±1.1	1.9±0.1	153.2±0.1	47.9±0.5	168.8±0.6	19.1±0.1
<i>PLA_1CNC-g-PLLA2</i>	60.3±0.3	32.0±0.1	98.6±0.3	3.3±0.5	154.9±0.1	50.4±0.1	168.0±0.1	16.4±0.4
<i>PLA_3CNC-g-PLLA2</i>	57.7±1.3	6.7±0.7	96.2±0.9	-	-	42.4±0.7	166.0±0.4	39.6±0.7

1

2 The analysis of thermodegradation products would give further insights on the occurring
3 thermodegradation pathways. Accordingly, the normalized spectra (according to CO₂ absorption
4 band, 2362 cm⁻¹) corresponding to exhaust gases obtained during the maximum rate of thermal
5 degradation for raw CNC, CNC-g-PLLA1, CNC-g-PLLA2 and their PLA based bionanocomposite
6 films are shown in Fig. 4. **Figure 4a shows the relative weight of PLA and the nanocomposites films
7 based on CNC at different content. It is evident that the CNC presence and content do not affect the
8 thermal degradation behaviour.** During thermodegradation of the neat PLA, methyl alcohol (broad
9 band at 3150-2650 cm⁻¹ and sharper one at 1100-950 cm⁻¹), carbon monoxide (2176 cm⁻¹ and 2120
10 cm⁻¹), carbon dioxide (2362 cm⁻¹, 2334 cm⁻¹ and 669 cm⁻¹) and water were released (McNeill &
11 Leiper. 1985; Zou, Yi, Wang, Liu, & Xu, 2009). On the contrary, as a result of cleavage of the
12 glycosidic linkages, the thermal degradation of raw CNC yields mainly CO₂, water (multiple peaks
13 in between 1900-1300 cm⁻¹), and CO compounds (Bourbigot, Chlebicki, & Mamleev, 2002).

14 The spectrum corresponding to CNC-g-PLLA1 is fairly similar to that obtained for raw CNC, while
15 the CNC-g-PLLA2 thermodegradation yields acetaldehyde (broad band at 2733 cm⁻¹ and shaper
16 ones at 1759 cm⁻¹, 1370 cm⁻¹ and 1106 cm⁻¹), CO₂, CO and water, which are characteristic of the
17 thermal degradation of polylactides (McNeill & Leiper. 1985). Obtained spectra suggest that CNC-
18 g-PLLA1 is mainly composed by cellulose, while CNC-g-PLLA2 presents large polylactide
19 fractions. This difference results in rather different thermodegradation pathways of
20 bionanocomposite films. In comparison with PLA_3CNC-g-PLLA1 bionanocomposite, the addition

1 of 3wt.% of CNC-g-PLLA2 to PLA matrix resulted in the development of larger quantities of CO
2 (intensity increase of 2176 cm^{-1} and 2120 cm^{-1} peaks) and water. Both bionanocomposites released
3 methyl alcohol and acetaldehyde during their thermodegradation (3200-2600 cm^{-1}), although the
4 presence of acetaldehyde was larger in the case of PLA_3CNC-g-PLLA2 as denoted by the increase
5 in 2740 cm^{-1} band. Moreover, acetaldehyde/ CO_2 ratio (estimated from 2362/1759 ratio), shifted
6 from 0.66 for PLLA_CNC-g-PLLA1 to 1.3 for PLLA_CNC-g-PLLA2 bionanocomposite. In
7 overall, those changes could be attributed to the differences on the amount of grafted PLLA chains
8 in CNC-g-PLLA1 and CNC-g-PLLA2 nanohybrids.

9

10 **3.2.4. X-ray diffraction**

11 Fig. 5a shows wide angle X-ray diffraction (WAXD) spectra of synthesized raw CNC, CNC-g-
12 PLLA1, CNC-g-PLLA2 and their PLA based bionanocomposite films. It is observed that raw CNC
13 presents three main peaks located at 15.7°, 22.5° and 35° corresponding to (101), (002) and (040)
14 planes of CNC crystal lattice respectively (Park, Baker, Himmel, Parilla, & Johnson. 2010). It is
15 important to emphasize that WAXD patterns of grafted CNC greatly differ from each other. While
16 CNC-g-PLLA1 only showed the characteristic diffraction peaks corresponding to crystalline
17 cellulose, CNC-g-PLLA2 showed featured reflections of PLLA orthorhombic form corresponding
18 to (010), (110)/(200), (203) and (015) planes achieved at $2\theta=14.8^\circ$, 16.8° , 19.2° and 22.3° ,
19 respectively (Kobayashi, et al., 1995). Those data suggested that the presence of grafted PLLA
20 chains in the synthesized CNC-g-PLLA1 was very low in comparison with CNC-g-PLLA2.
21 Additionally, it resulted reasonable to suppose that the rather low molecular weight of PLLA chains
22 in CNC-g-PLLA2 nanohybrid (as evidenced by its low melting temperature of 158 °C) confers high
23 crystallization ability to attached chains.

24 Although all fabricated bionanocomposite films presented a broad halo centered at $2\theta\sim 16^\circ$ denoting
25 a predominantly amorphous microstructure of specimens, its height slightly increased for

1 bionanocomposites containing 3 wt.% of both CNC-g-PLLA. This increased intensity was ascribed
2 to the development of ordered regions during the filmature process, which agrees well with
3 obtained DSC data where it is shown that the crystallinity degree increases from 12.8 % for neat
4 PLA to 18.6 % for its PLA_3CNC-g-PLLA2 bionanocomposite (see Table 2). In order to confirm
5 the presence of CNC within the fabricated films, further WAXD experiments were carried out for
6 longer times. Fig. 5b displays obtained diffraction patterns for bionanocomposites containing 3
7 wt.% within the $2\theta=8-28^\circ$ region (neat CNC pattern is shown for comparison). It was observed that
8 besides of the predominant main amorphous halo, both PLA_3CNC-g-PLLA1 and PLA_3CNC-g-
9 PLLA2 bionanocomposites presented a small shoulder located at $2\theta=22.5^\circ$ corresponding to the
10 (002) plane of CNC crystal lattice, which certified the presence of cellulosic crystals within the
11 films.

12

13 **3.2.5. Infrared Spectroscopy**

14 The FT-IR spectra of (c) PLA-CNC-g-PLLA1 and (d) PLA-CNC-g-PLLA2 films are presented in
15 Fig. 5. This analysis attempts to characterize the incorporation of CNC-g-PLLA nanohybrids in
16 PLA based films and distinguish the infrared bands and vibration shifts related to interactions. The
17 absorption peaks of the bionanocomposite spectrum were mainly due to the $-\text{CH}_3$ stretching
18 vibration at 2990 cm^{-1} . A strong absorption band was observed at 1757 cm^{-1} due to the C=O
19 stretching from keto esters. The sample with CNC-g-PLLA1 showed an increased absorption peak
20 between $3300-3400\text{ cm}^{-1}$ due to the CNC presence in the film, as underlined in the Fig. 1b. As the
21 CNC-g-PLLA content was increased from 1 wt.% to 3 wt.%, the stretching vibrations of OH groups
22 of cellulose increased gradually. Spectra showed the typical features of cellulose, the broad bands in
23 the $3650-3000\text{ cm}^{-1}$ region are due to O-H stretching vibrations. The bending vibrations at 1452
24 and 1382 cm^{-1} were due to the antisymmetric and symmetric deformations of $-\text{CH}_3$ group, as
25 already reported by Pamula et al. 2001 (Pamula, et al. 2001) in the region $1300-1500\text{ cm}^{-1}$. The
26 bands at 1266 and 1189 cm^{-1} were related to the antisymmetric and symmetric stretching of C-O-C

1 in esters. The peak at 1181 cm^{-1} could be attributed to C–O–C stretching of PLA (Molinaro, et al.
2 2013) and the peaks at 1125 , 1080 and 1040 cm^{-1} may correspond to C–O stretching vibrations
3 (Pamula, et al. 2001). The bands detected at 868 and 755 cm^{-1} (far infrared) can be assigned,
4 respectively, to the amorphous and crystalline phases of PLA (Molinaro, et al. 2013).

5

6 **3.2.6. Mechanical Properties**

7 Fig. 6 depicts the stress-strain curves of raw PLA and its bionanocomposites, while the main
8 representative mechanical parameters are summarized in Table 1. Neat polymer presented a stiff
9 and semi-ductile behaviour with a strain at yield (ϵ_y) of 2.6% and strain at break (ϵ_b) of 5.6%. As a
10 general rule, tensile modulus was continuously increased at expenses of ductility upon CNC-g-
11 PLLA nanohybrids loading. Those changes were especially noticeable for the PLA_CNC-g-PLLA2
12 nanocomposites, where the Young's modulus increases by 23 % with the addition of 3 wt.% of
13 cellulose nanocrystals. Surprisingly, the elongation at break of PLA_1CNC-g-PLLA1 was increased
14 from 5.6 % up to 9.5 %, which may be attributed to the increased dispersion and interfacial
15 adhesion provided by the grafted PLLA chains (Lönnberg, Larsson, Lindström, Hult, &
16 Malmström, 2011; Lin, Chen, Huang, Dufresne, & Chang, 2009). More precisely, it has been
17 previously suggested that grafted chains create a co-continuous phase in which local stresses are
18 evenly transferred to the remaining PLA phase, which in turn improved the mechanical properties
19 of the bulk material (Cao, Habibi, & Lucia, 2009).

20 Fig. 6b compares the experimentally obtained data and predicted Young's modulus values according
21 to random Halpin-Tsai equation. It is noticed that the experimental values remained below the
22 predicted data, which is especially noticeable at high concentrations and for the PLA_CNC-g-
23 PLLA1 system. The fact that the Young's modulus of PLA_1CNC-g-PLLA2 (corresponding to a
24 volume fraction of 0.75%) fits rather well may be ascribed to an effective stress transfer across the
25 CNC-to-PLA interface together with a good CNC distribution over the entire bionanocomposite

1 (Choudhury, 2014). However, it could be concluded from the overprediction of tensile modulus that
2 other formulations yield a non-homogeneous aggregated morphology.

3

44. Conclusions

5 Cellulose nanocrystals were subjected to surface grafting of poly(L-lactide) through ring opening
6 polymerization initiated from the hydroxyl groups available on their surface.

7 The resulting CNC-g-PLLA nanohybrids were successfully incorporated in poly(lactic acid)
8 polymer matrix through melt-blending. The effect of cellulose modification and amount in the
9 bionanocomposites was deeply characterized in terms of their **morphological, optical and thermo-**
10 **mechanical properties.**

11 The **CNC:L-lactide ratios affect** the grafting efficiency and, consequently, the bionanocomposite
12 thermal, mechanical and optical properties.

13 **Microstructure analysis and optical properties underlined a good dispersion of cellulose**
14 **nanocrystals in the polymer matrix. Thermal properties highlighted the best efficiency in the**
15 **samples with the highest content of CNC-g-PLLA2 (3 wt.%). Tensile modulus was increased with**
16 **the CNC introduction, as expected, while the elongation at break of PLA_1CNC-g-PLLA1 was**
17 **improved of the 70% respect to PLA polymer matrix film.**

18 Acknowledgements

19 E.L. thanks the University of the Basque Country (UPV/EHU) for a postdoctoral fellowship. We
20 gratefully acknowledge Corbion-Purac for the kind donation of L-lactide monomer and PLLA.
21 Technical and human support provided by SGIker (UPV/EHU, MICINN, GV/EJ, EGEF, and ESF)
22 is gratefully acknowledged.

23

245. References

- 1 Arias, A., Heuzey, M.C., Huneault, M.A., Ausias, G., Bendahou, A. (2015). Enhanced dispersion of
2 cellulose nanocrystals in melt-processed polylactide-based nanocomposites. *Cellulose*, 22,
3 483-498.
- 4 Armentano, I., Bitnis, N., Fortunati, S., Rescignano, N., Verdejo, R., Lopez-Manchado, M. A., et al.
5 (2013). Multifunctional nanostructured PLA materials for packaging and tissue engineering.
6 *Progress in Polymer Science*, 38(10-11), 1720-1747.
- 7 Auras, R. Harte, & B. Selke, S. (2004). An overview of polylactides as packaging materials.
8 *Macromolecular Bioscience*, 4, 835-864.
- 9 Bitinis, N., Verdejo, R., Bras, J., Fortunati, E. Kenny, J.M., Torre, L., et al. (2013) Poly(lactic
10 acid)/natural rubber/cellulose nanocrystal bionanocomposites Part I. Processing and
11 morphology *Carbohydrate Polymers*, 96, 611–620.
- 12 Bourbigot, S., Chlebicki, S., & Mamleev, V. (2002). Thermal degradation of cotton under linear
13 heating. *Polymer Degradation and Stability*, 78, 57-62.
- 14 Cao, X., Habibi, Y., & Lucia, L. A. (2009). One-pot polymerization, surface grafting, and
15 processing of waterborne polyurethane-cellulose nanocrystal nanocomposites. *Journal of*
16 *Materials Chemistry*, 19, 7137–7145.
- 17 Choudhury A. (2014). Preparation and characterization of nanocomposites of poly-p-phenylene
18 benzobisthiazole with graphene nanosheets. *RSC Advances*, 4, 8856-8866.
- 19 CIE, 1995 Industrial colour-difference evaluation. Technical report 116/1995 ed. Commission
20 Internationale de l'Éclairage Central Bureau, Wien, Austria.
- 21 Colom, X., & Carrillo, F. (2002). Crystallinity changes in lyocell and viscosetype fibres by caustic
22 treatment. *European Polymer Journal*, 38, 2225–2230.

- 1 Dechy-Cabaret, O., Martin-Vaca, B., & Bourissou, D. (2004). Controlled Ring-Opening
2 Polymerization of Lactide and Glycolide. *Chemical Reviews*, 104, 6147–6176.
- 3 Diddens, I., Murphy, B., Krisch, M., & Muller, M. (2008). Anisotropic elastic properties of
4 cellulose measured using inelastic X-ray scattering. *Macromolecules*, 41, 9755–9759.
- 5 Dufresne, A. (2013). Nanocellulose: a new ageless bionanomaterial. *Materials Today*, 16, 220-227.
- 6 Fortunati, E., Armentano, I., Zhou, Q., Iannoni, A., Saino, E., Visai, L., Berglund, L.A., & Kenny,
7 J.M. (2012)a. Multifunctional bionanocomposite films of poly(lactic acid), cellulose
8 nanocrystals and silver nanoparticles. *Carbohydrate Polymers*, 87, 1596-1605.
- 9 Fortunati, E., Armentano, I., Zhou, Q., Puglia, D., Terenzi, A., Berglund, L.A., & Kenny, J.M.
10 (2012)b. Microstructure and nonisothermal cold crystallization of PLA composites based on
11 silver nanoparticles and nanocrystalline cellulose. *Polymer Degradation and Stability*, 97,
12 2027–2036.
- 13 Goffin, A. L., Raquez, J. M., Duquesne, E., Siqueira, G., Habibi, Y., Dufresne, A. et al. (2011)
14 From interfacial ring-opening polymerization to melt processing of cellulose nanowhisker
15 filled polylactide based nanocomposites. *Biomacromolecules*, 12, 2456-2465.
- 16 Goncalves, C. M. B., Cuntinho, J. A. P., & Marrucho, I. M. (2010). In R. A. Auras, L. T.Lim, & S.
17 E. M. Selke, et al. (Eds.), *Poly(lactic acid): Synthesis, structures, properties, processing and*
18 *applications*. (pp. 97–112). Hoboken, NJ: John Wiley & Sons, Inc.
- 19 Habibi, Y., Aouadi, S., Raquez, J.M., & Dubois, P., (2013) Effects of interfacial stereocomplexation
20 in cellulose nanocrystal-filled polylactide nanocomposites. *Cellulose*, 20, 2877–2885.
- 21 Habibi, Y. (2014) Key advances in the chemical modification of nanocelluloses. *Chemical Society*
22 *Reviews*, 43, 1519.

- 1 Halpin, J.C., & Kardos, J.L. (1976). The Halpin-Tsai equations: a review. *Polymer Engineering and*
2 *Science*, 16, 344-352.
- 3 Hui, C.Y., & Shia, D. (1998). Simple formulae for the effective moduli of unidirectional aligned
4 composites. *Polymer Engineering and Science*, 38, 774-782.
- 5 Kobayashi, J., Asahi, T., Ichiki, M., Oikawa, A., Suzuki, H., Watanbe, T., Fukada, E., & Shikinami,
6 Y. (1995). Structural and optical properties of poly lactic acids. *Journal of Applied Physiscs*,
7 77, 2957-2973.
- 8 Kondo, T., & Sawatari, C. (1996). A Fourier transform infrared spectroscopic analysis of the
9 character of hydrogen bonds in amorphous cellulose. *Polymer*, 37, 393–399.
- 10 Lin, N., Chen, G., Huang, J., Dufresne, A., & Chang, P.R. (2009). Effects of polymergrafted natural
11 nanocrystals on the structure and mechanical properties of poly(lactic acid): a case of
12 cellulose whisker-graft polycaprolactone. *Journal of Applied Polymer Science*, 113(5), 3417–
13 25.
- 14 Liu, G., Zhang, X., & Wang, D. (2014) Tailoring Crystallization: Towards High-Performance
15 Poly(lactic acid). *Advanced Materials*, 26(40), 6905-6911.
- 16 Lizundia, E., Petisco, S., & Sarasua, J. R. (2013). Phase-structure and mechanical properties of
17 isothermally melt-and cold-crystallized poly (L-lactide). *Journal of the Mechanical*
18 *Behavior of Biomedical Materials*, 17, 242-251.
- 19 Lizundia, E., Meaurio, E., Laza, J. M., Vilas, J. L., & León, L. M. (2015). Study of the chain
20 microstructure effects on the resulting thermal properties of Poly(L-lactide)/Poly(N-
21 isopropylacrylamide) biomedical materials. *Materials Science and Engineering C: Materials*
22 *for Biological Applications*, 50, 97-106.

- 1 Lizundia, E., Vilas, J.L., & León, L.M. (2015). Crystallization, structural relaxation and thermal
2 degradation in Poly(L-lactide)/cellulose nanocrystal renewable nanocomposites.
3 *Carbohydrate Polymers*, 123, 256–265.
- 4 Lönnerberg, H., Larsson, K., Lindström, T., Hult, A., & Malmström, E. (2011). Synthesis of
5 polycaprolactone-grafted microfibrillated cellulose for use in novel bionanocomposites-
6 influence of the graft length on the mechanical properties. *ACS Applied Materials and*
7 *Interfaces*, 3(5), 1426–1433.
- 8 Martin, O. & Avérous. (2001). Poly(lactic acid): plasticization and properties of biodegradable
9 multiphase systems. *Polymer*, 42(14), 6209-6219.
- 10 McNeill I. C., & Leiper, H. A. (1985). Degradation studies of some polyesters and polycarbonates-
11 1. Polylactide: General features of the degradation under programmed heating conditions.
12 *Polymer Degradation and Stability*, 11, 267-285;
- 13 Meaurio, E., Martinez de Arenaza, I., Lizundia, E., & Sarasua, J. R. (2009). Analysis of the C=O
14 stretching band of the α -crystal of Poly(L-lactide). *Macromolecules*, 42, 5717–5727
- 15 Molinaro, S., Romero, M.C., Boaro, M., Sensidoni, A., Lagazio, C., Morris, M., & Kerry, J. (2013).
16 Effect of nanoclay-type and PLA optical purity on the characteristics of PLA-based
17 nanocomposite films. *Journal of Food Engineering*, 117, 113–123.
- 18 Obarzanek-Fojt, M., Elbs-Glatz, Y., Lizundia, E., Diener, L., Sarasua, J. R., & Bruinink, A. (2014).
19 From implantation to degradation — are poly (l-lactide)/multiwall carbon nanotube
20 composite materials really cytocompatible?. *Nanomedicine: Nanotechnology, Biology and*
21 *Medicine*, 10(5), 1041-1051.

- 1 Oh, S. Y., Yoo, D. I., Shin, Y., Kim, H. C., Kim, H. Y., Chung, Y. S., et al. (2005). Crystalline
2 structure analysis of cellulose treated with sodium hydroxide and carbon dioxide by means
3 of X-ray diffraction and FTIR spectroscopy. *Carbohydrate Research*, 340, 2376–2391.
- 4 Pamula, E., Błażewicz, M., Paluszkiewicz, C., & Dobrzyński, P. (2001). FTIR study of degradation
5 products of aliphatic polyesters–carbon fibres composites. *Journal of Molecular Structure*,
6 596, 369–75.
- 7 Park, S., Baker, J. O., Himmel, M. E., Parilla, P. A., & Johnson, D. K. (2010). Cellulose
8 crystallinity index: measurement techniques and their impact on interpreting cellulase
9 performance. *Biotechnology for Biofuels*, 3, 10.
- 10 Paul, D. R., & Robeson, L. M. (2008). Polymer nanotechnology: Nanocomposites, *Polymer*, 49(15),
11 3187-3204;
- 12 Roman, M., & Winter, W. T. (2004). Effect of sulfate groups from sulfuric acid hydrolysis on the
13 thermal degradation behavior of bacterial cellulose. *Biomacromolecules*, 5, 1671–1677.
- 14 Rusli, R., & Eichhorn, S.J. (2008). Determination of the stiffness of cellulose nanowhiskers and the
15 fiber-matrix interface in a nanocomposite using Raman spectroscopy. *Applied Physics*
16 *Letters*, 93, 033111.
- 17 Song, Z., Xiao, H., & Zhao, Y. (2014). Hydrophobic-modified nano-cellulose fiber/PLA
18 biodegradable composites for lowering water vapor transmission rate (WVTR) of paper.
19 *Carbohydrate Polymers*, 111, 442–448.
- 20 Sonjui, T., & Jiratumnukul, (2014). Poly (lactic acid) organoclay nano composites for paper coating
21 applications. *Songklanakarin J. Sci. Technol.* 536 36 (5), 535-540.

- 1 Spinella, S., Lo Re, G., Liu, B., Dorgan, J., Habibi, Y., Leclere, P., et al. (2015).
2 Polylactide/cellulose nanocrystal nanocomposites: Efficient routes for nanofiber
3 modification and effects of nanofiber chemistry on PLA reinforcement. *Polymer*, 65, 9-17.
- 4 Turhan, K. N., & Sahbaz, F. (2001). A simple method for determining light transmittance of
5 polymer films used for packaging foods. *Polymer International*, 50, 1138.
- 6 Xiao, S., Gao, R., Lu, Y., Li, L., & Sun, Q. (2015). Fabrication and characterization of
7 nanofibrillated cellulose and its aerogels from natural pine needles. *Carbohydrate Polymers*,
8 119, 202–209.
- 9 Yang, W. Dominici, F., Fortunati, E., Kenny, J.M., & Puglia, D. (2015). Melt free radical grafting
10 of glycidyl methacrylate (GMA) onto fully biodegradable poly(lactic) acid films: effect of
11 cellulose nanocrystals and a masterbatch process. *RSC Advances*, 5, 32350-32357.
- 12 Zou, H., Yi, C., Wang, L., Liu, H., & Xu, W. (2009). Thermal degradation of poly(lactic acid)
13 measured by thermogravimetry coupled to Fourier transform infrared spectroscopy. *Journal*
14 *of Thermal Analysis and Calorimetry*, 97, 929-935.

15

16 **Figure and Table Captions**

17 **Fig. 1.** a) TEM image showing synthesized cellulose nanocrystals; b) FT-IR spectra of neat CNC
18 and CNC-g-PLLA nanohybrids; c) DSC traces obtained after quenching samples from the melt of
19 synthesized CNC-g-PLLA nanohybrids and d) TGA of raw CNC and CNC-g-PLLA.

20 **Fig. 2.** FESEM micrographs of cryogenically fractured surfaces of PLA and PLA
21 bionanocomposites: a) PLA; b) PLA_1CNC-g-PLLA1; c) PLA_3CNC-g-PLLA1; d) PLA_1CNC-
22 g-PLLA2 and e) PLA_3CNC-g-PLLA2.

23 **Fig. 3.** DSC traces of neat PLA and its bionanocomposites obtained during: a) first heating scan; b)
24 cooling from the melt and c) second heating scan.

25 **Fig. 4.** a) Thermogravimetric traces of neat PLA and its bionanocomposite counterparts and b) FT-
26 IR spectra of thermodegradation products obtained at the maximum weight loss.

1 **Fig. 5.** a) XRD patterns of synthesized CNC, CNC-g-PLLA nanosystems and its 1wt.% and 3 wt.%
2 nanocomposite counterparts and b) enlarged XRD patterns within the 2θ 8-28° region . FT-IR
3 spectra of c) PLA-CNC-g-PLLA1 and d) PLA-CNC-g-PLLA2 films.

4 **Fig. 6.** a) Representative stress-strain diagrams of neat PLA and PLA bionanocomposites and b)
5 experimental data and fitting results of neat PLA and PLA_CNC-g-PLLA bionanocomposites.

6 **Table 1.** Apparent color, gloss and mechanical properties of PLA and PLA bionanocomposite
7 films.

8 **Table 2.** Thermal properties from DSC analysis of PLA and PLA bionanocomposite films from the
9 first and the second heating scan.

Figure 1
[Click here to download high resolution image](#)

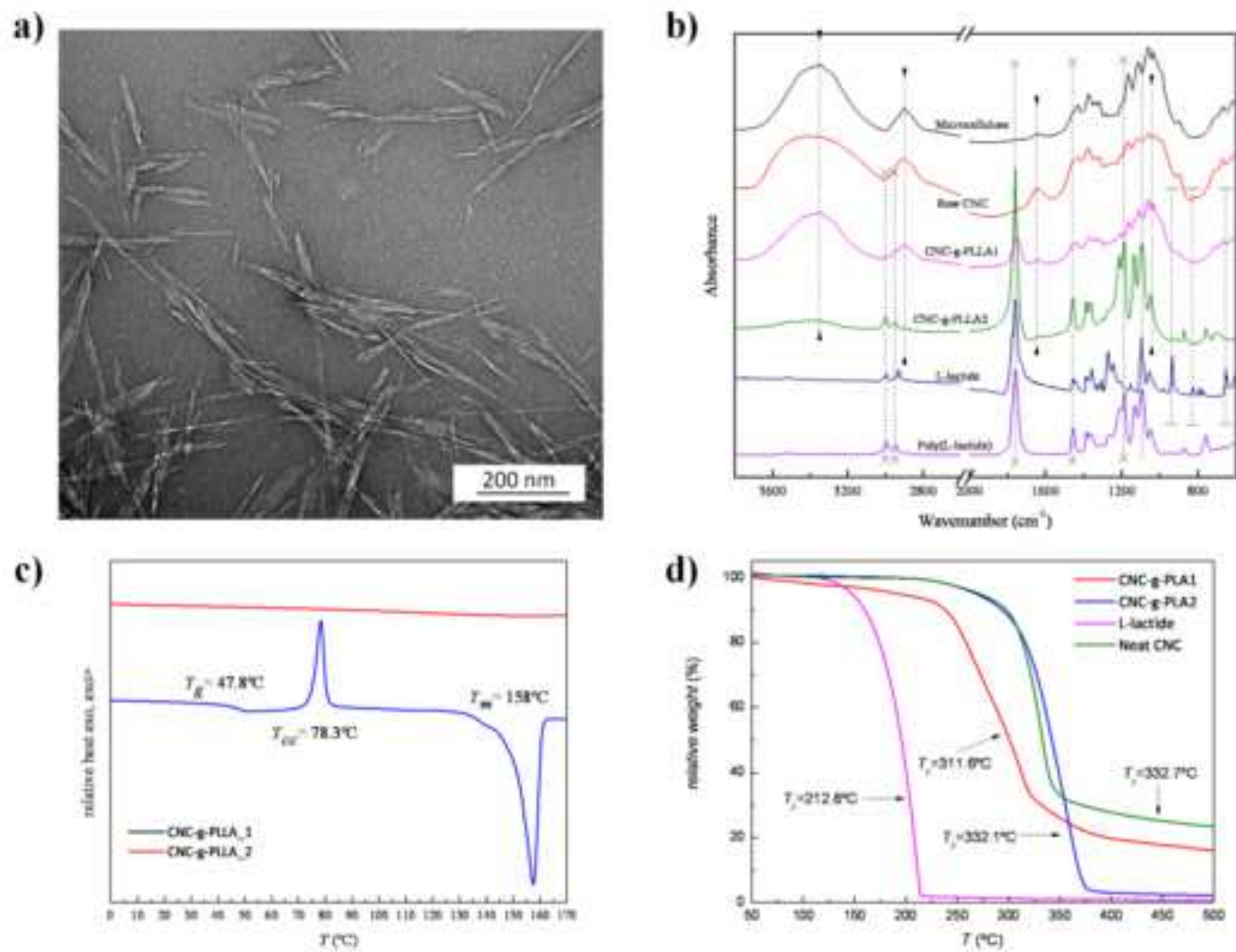


Figure 2
[Click here to download high resolution image](#)

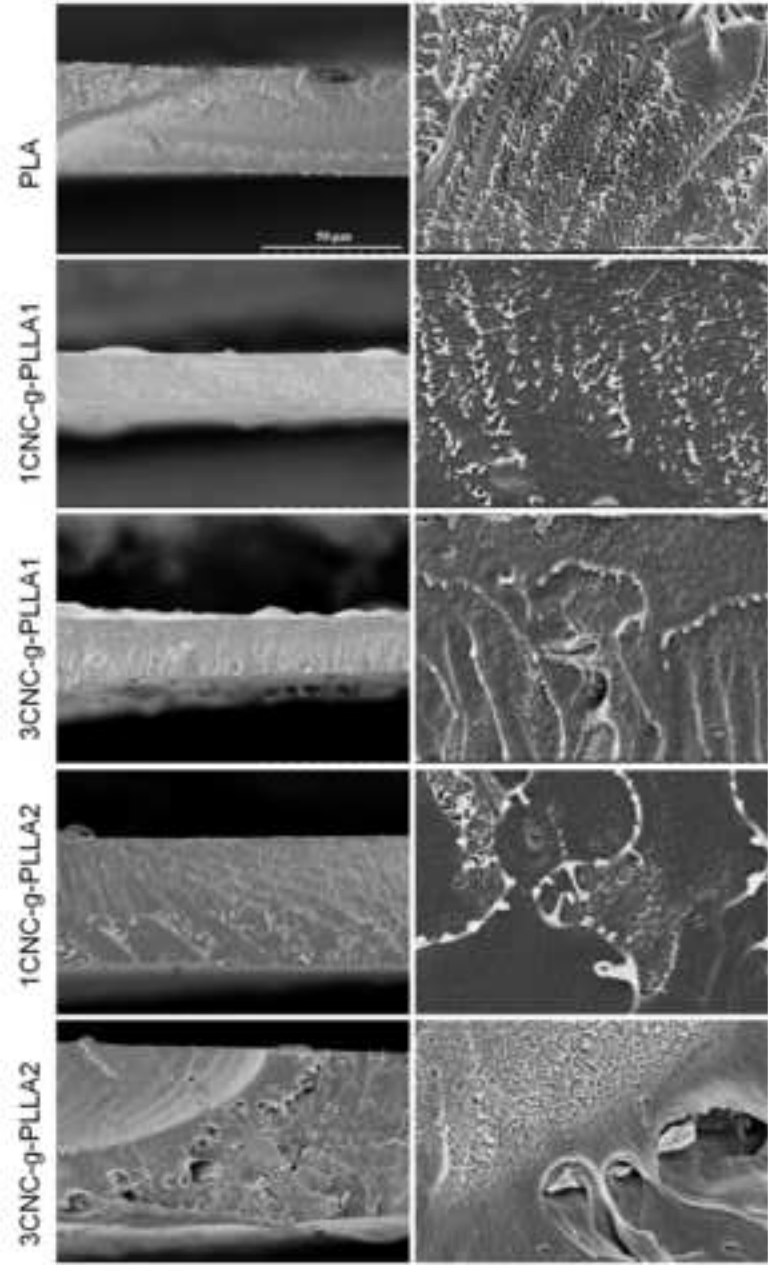


Figure 3
[Click here to download high resolution image](#)

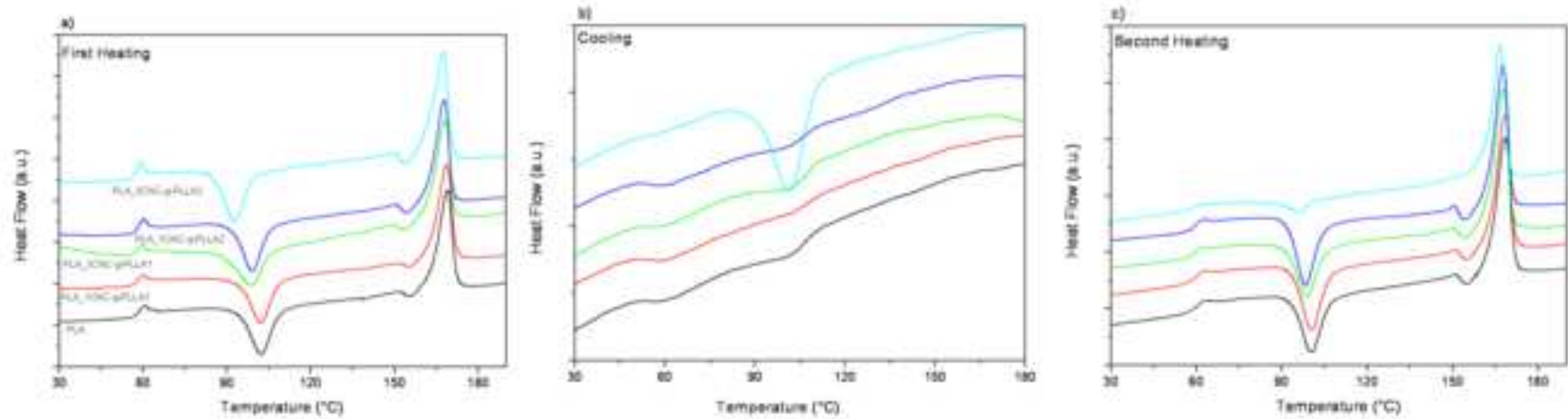


Figure 4
[Click here to download high resolution image](#)

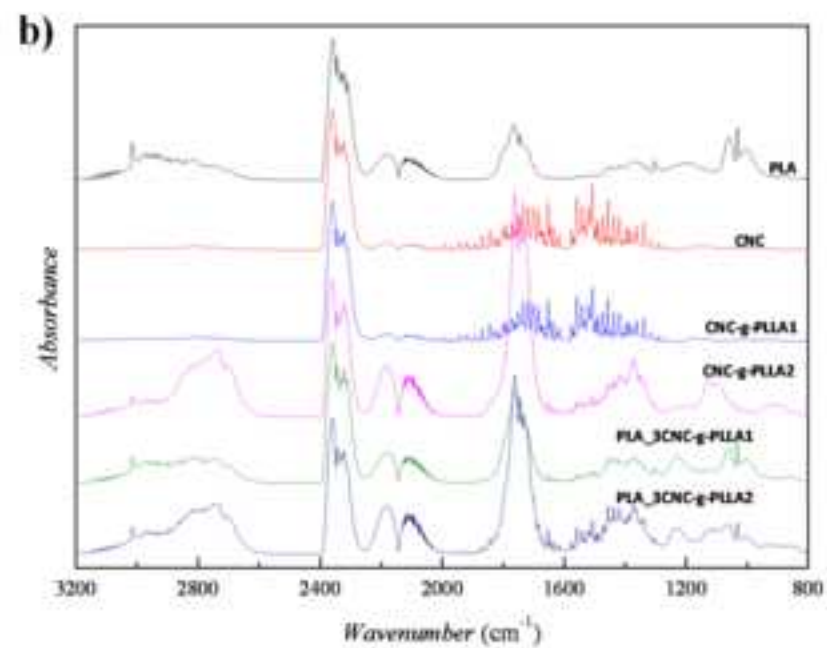
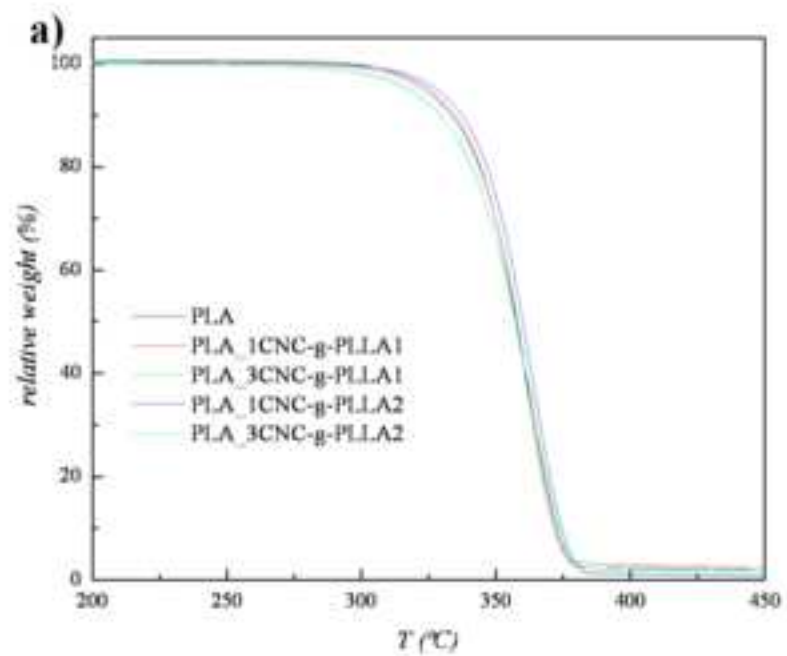


Figure 5
[Click here to download high resolution image](#)

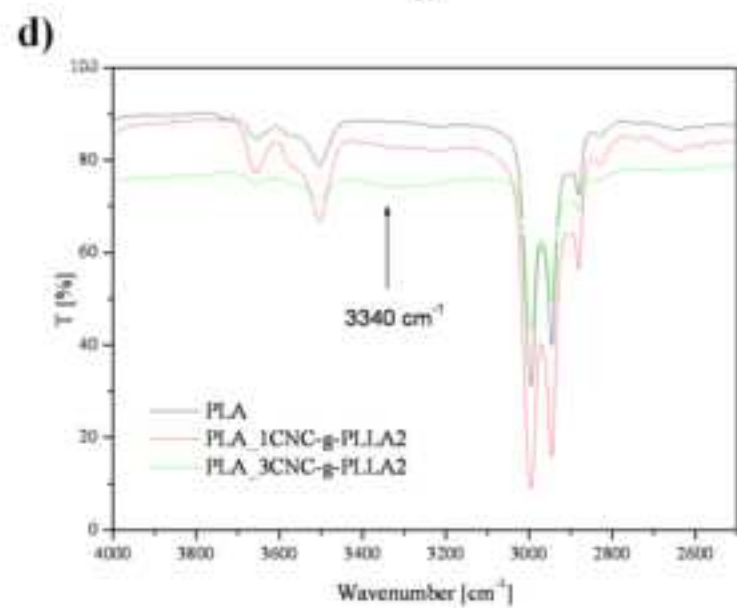
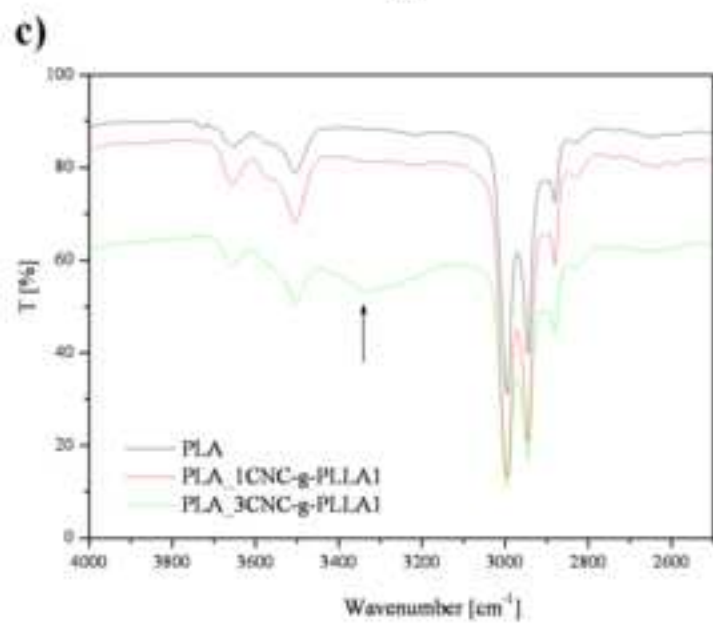
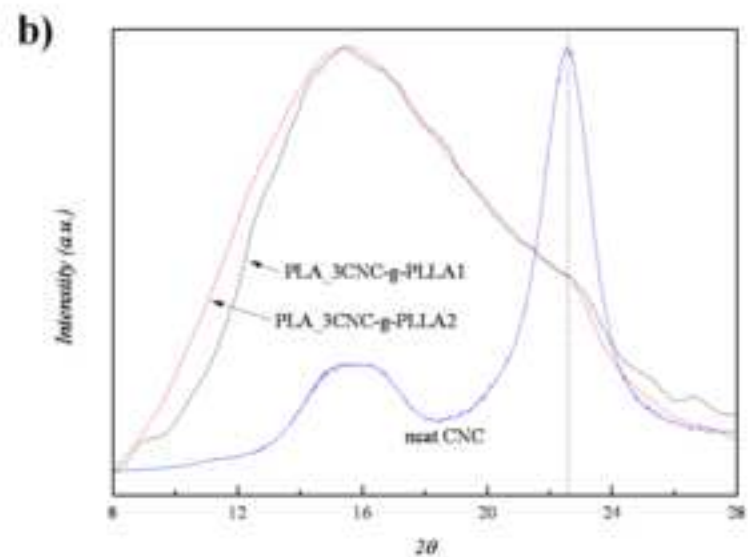
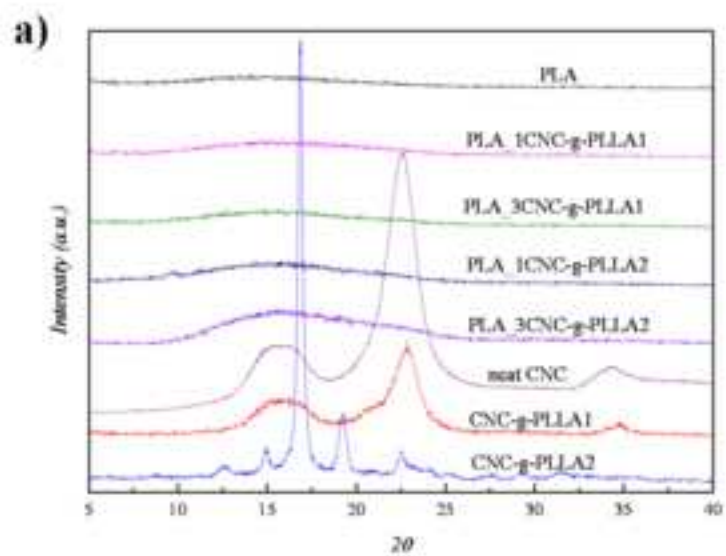


Figure 6
[Click here to download high resolution image](#)

